

# Intrinsic dimension estimation for discrete metrics

Iuri Macocco,<sup>1</sup> Aldo Glielmo,<sup>1,2</sup> Jacopo Grilli,<sup>3</sup> and Alessandro Laio<sup>1,3, a)</sup>

<sup>1)</sup>International School for Advanced Studies (SISSA), Via Bonomea 265, 34136 Trieste, Italy

<sup>2)</sup>Banca d'Italia, Italy<sup>b)</sup>

<sup>3)</sup>The Abdus Salam International Centre for Theoretical Physics (ICTP), Strada Costiera 11, 34014 Trieste, Italy

Real world-datasets characterized by discrete features are ubiquitous: from categorical surveys to clinical questionnaires, from unweighted networks to DNA sequences. Nevertheless, the most common unsupervised dimensional reduction methods are designed for continuous spaces, and their use for discrete spaces can lead to errors and biases. In this letter we introduce an algorithm to infer the intrinsic dimension (ID) of datasets embedded in discrete spaces. We demonstrate its accuracy on benchmark datasets, and we apply it to analyze a metagenomic dataset for species fingerprinting, finding a surprisingly small ID, of order 2. This suggests that evolutive pressure acts on a low-dimensional manifold despite the high-dimensionality of sequences' space.

Real-world data are often defined by a very large number of features, but are effectively contained in a manifold which can be described, at least locally, by a relatively small number of coordinates. Such number is called Intrinsic Dimension (ID). The ID is the minimum number of variables needed to describe the data without significant information loss. Its knowledge is of paramount importance in unsupervised learning<sup>1-3</sup>. In solid state physics and statistical physics the ID can be used as a proxy of an order parameter describing phase transitions<sup>4,5</sup>; in molecular dynamics it can be used to quantify the complexity of a trajectory<sup>6</sup>; in deep learning theory, the ID indicates how information is compressed throughout the various layers of a network<sup>7-9</sup>. During the last three decades, there have been many progress in the development of sophisticated tools aimed at inferring the ID<sup>10,11</sup> but, to our knowledge, all present estimators have been formulated (and are supposed to work) in spaces where distances can vary continuously. However, many systems are characterised by discrete features and, consequently, discrete distances. For instance, categorical datasets like satisfaction questionnaires, clinical trials, unweighted networks, spin systems, protein and DNA sequences fall in this category. The application of ID estimators developed for continuous features to discrete features brings in approximations as the theory behind the method is grounded in a different domain. The obtained estimates can be affected by systematic errors that, possibly, are negligible only in the limit of low density data-points, where the discrete structure becomes less relevant.

In this letter, we introduce an ID estimator explicitly formulated for spaces with discrete features. In discrete spaces, the ID can be thought of as the dimension of a (hyper)cubic lattice where the original data-points can be (locally) projected without a significant information loss.

Working with discrete data poses two main conceptual and technical difficulties. The first one is degeneracy: one can have multiple points that lie at the same exact distance from each other, or even at zero distance. This problem is entangled with a second one: many ID estimators assume that the number of data in the neighborhood of a point should scale with a power law of the radius of the neighborhood<sup>12</sup>. In a discrete space, this relationship does not hold, not even as an approximation, especially for small distances. The key idea which we introduce here is that, in order to deal with the discrete nature of the data one should properly define volumes on lattices. To do this, we use Ehrhart's theory of polytopes<sup>13</sup>, that allows to enumerate the lattice points of a given region. By measuring a suitable statistics depending on the number of data-points observed within a given (discrete) distance, one can infer the value of the dimension of the region, which we interpret as the ID of the dataset. The statistics we use is defined in such a way that density of points is required to be constant only locally and not in the whole dataset. Importantly, our estimator allows to explicitly select the scale at which the ID is computed.

*Methods* - We assume data points to be uniformly distributed on a generic domain, and that their density is  $\rho$ . In such domain, we consider a region  $A$  with volume  $V(A)$ . Since we are assuming points to be independently generated, the probability of observing  $n$  points in  $A$  is given by the Poisson distribution<sup>14</sup>

$$P(n, A) = \frac{[\rho V(A)]^n}{n!} e^{-\rho V(A)} \quad (1)$$

so that  $\langle n \rangle = \rho V(A)$ . Consider now a data-point  $i$  and two regions  $A$  and  $B$ , one containing the other, and both containing the data-point:  $i \in A \subset B$ . Then the number of points  $n$  and  $k - n$  falling, respectively, in  $A$  and  $B \setminus A$  are Poisson distributed with rates  $\lambda_1 = \rho V(A)$  and  $\lambda_2 = \rho V(B \setminus A)$ . The conditional probability of having  $n$  points in  $A$  given that there are  $k$  points in  $B$  is

$$P(n | k) = \frac{P(n)P(k-n)}{P(k)} = \binom{k}{n} p^n (1-p)^{k-n} \quad (2)$$

<sup>a)</sup>Electronic mail: laio@sissa.it

<sup>b)</sup>The views and opinions expressed in this paper are those of the authors and do not necessarily reflect the official policy or position of Banca d'Italia.

with

$$p = \frac{\lambda_1}{\lambda_1 + \lambda_2} = \frac{\rho V(A)}{\rho V(B)} = \frac{V(A)}{V(B)}. \quad (3)$$

Thus  $n|k \sim \text{Binomial}(n; k, p)$ . As far as the density  $\rho$  is constant within  $A$  and  $B$ ,  $p$  is simply equal to the ratio of the volumes of the considered regions and, remarkably, density independent. This is a key property which, as we will show, allows using the estimator even when the density is approximately constant only locally, and varies, even substantially, across larger distance scales. One can then write a conditional probability of the observations  $n_i$  (one for each data point), given the parameters  $k_i$  and  $p_i$ , which can possibly be point-dependent:

$$\mathcal{L}(n_i|k_i, p_i) = \prod_{i=1}^N \text{Binomial}(n_i|k_i, p_i). \quad (4)$$

Such formulation assumes all the observations to be statistically independent. Strictly speaking this is typically not true, since the regions  $A$  and  $B$  of different points can be overlapping. We will address this issue in Supplementary Information (SI), demonstrating that neglecting correlations does not induce significant errors.

The next step consists in defining the volumes in Eq. (3) according to the nature of the embedding manifold. We now assume our space to be a lattice where the  $L^1$  metric is a natural choice. In this space the volume  $V(A)$  is the number of lattice points contained in  $A$  (see SI Fig.5). According to Ehrhart theory of polytopes<sup>15</sup>, the number of lattice points within distance  $t$  in dimension  $d$  from a given point amounts to<sup>16</sup>

$$V_{\diamond}(t, d) = \binom{d+t}{d} {}_2F_1(-d, -t, -d-t, -1) \quad (5)$$

where  ${}_2F_1(a, b, c, z)$  is the ordinary hypergeometric function. At a given  $t$ , the above expression is a polynomial in  $d$  of order  $t$  (see SI). As a consequence, the ratio of volumes defining the value of  $p$  in Eq. (3) becomes a ratio of two polynomials in  $d$ . Given a dataset, the choice of  $t_1$  and  $t_2$  fixes the values of  $n_i$  and  $k_i$  in the likelihood (4). Its maximization with respect to  $d$  allows to infer the ID of the data-manifold. This accounts to find the root of equation (see SI)

$$\frac{V_{\diamond}(t_1, d)}{V_{\diamond}(t_2, d)} - \frac{\langle n \rangle}{\langle k \rangle} = 0 \quad (6)$$

where the mean value over  $n$  and  $k$  is intended over all the points of the dataset. The root can be easily found with standard optimization libraries. This procedure defines an ID estimator that, for brevity, we will call I3D (Intrinsic Dimension estimator for Discrete Datasets).

Very importantly, the ID estimate is density independent as such factor cancels out (see Eq. (3)). The error on the estimator has a theoretical lower bound, given by the Cramer-Rao inequality, which has an explicit analytic expression (see SI). As an alternative, the ID can

be estimated by a Bayesian approach as the mean value of its posterior distribution, and the error estimated via the posterior variance (details in SI).

The estimation of the ID depends on the choice of the volumes of the smaller and larger regions, which are parametrised by the "radii"  $t_1$  and  $t_2$ . By varying  $t_2$ , the radius of the largest probe region, one can explore the behaviour of the ID at different scales. This leaves the procedure with one free parameter: the ratio  $r = t_1/t_2$  and its choice influences the statistical error. In continuous space the ratio between volumes in Eq. (3) is simply  $p = r^d$  and the Cramer-Rao variance has a simple dependence on the parameter  $r$ . By minimising it with respect to  $r$ , one obtains that the optimal value for the ratio is  $r_{opt} \sim 0.2032^{\frac{1}{d}}$  (see SI).

In order to check the goodness of the estimator we test whether the number of points  $n$  contained within the internal shells are actually distributed as a mixture of binomials, as our model assumes:

$$P(n) = \sum_k P(k) \text{B}(n; k, \frac{V_{\diamond}(t_1, d)}{V_{\diamond}(t_2, d)}) \quad (7)$$

where  $P(k)$  is the empirical probability distribution of the  $k$  found by fixing  $t_2$ . In the following we will compare the empirical cumulative distribution of  $n$  to the cumulative distribution of  $P(n)$ .

*Results: Uniform distribution* - We tested the I3D estimator on artificial datasets, and compared it against "two nearest neighbours" (2nn)<sup>17</sup>, an ID estimator conceived for continuous-valued datasets. We started by analysing uniformly-distributed points in 2d and 6d square lattices. We adopted periodic boundary conditions in order to reduce boundary effects as much as possible. For the I3D estimator, in this and all following cases, we set  $t_1/t_2 = r = 0.5$ . Results are shown in Fig. 1. The lattice structure, together with the high density and the consequent possible overlap of some points, prevents 2nn from providing a precise estimate. The correct ID is obtained only under aggressive decimation of the dataset. The I3D estimator, instead, returns accurate values for the ID at all scales. It has to be noticed that, while for the computation with 2nn we had to explicitly eliminate overlapping points to avoid divergences, such operation was not necessary for the I3D estimator, as it can perfectly deal with possible degeneracies. The large error bars (given by the standard deviation over the different realizations) for low values of  $t_2$  in the 6d case are related to the low number of points found at such distances. Remarkably, the I3D estimator allows to select the scale explicitly by varying the radius  $t_1$ . On the other hand, the scale at which 2nn is just the average distance of the second neighbour, and is therefore different in different points and cannot be controlled directly. In Fig. 1, lower panels, we also report a first example of model validation. The two cdfs (empirical and theoretical one, according to Eq. (7)) perfectly match, meaning that the ID estimation is reliable.

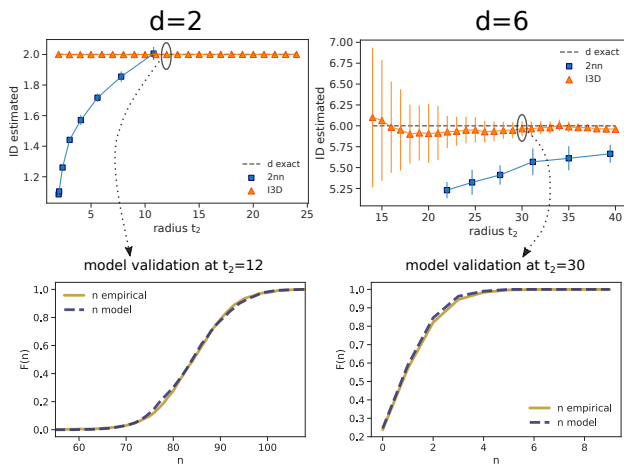


FIG. 1. Performance of I3D and 2nn estimators for points uniformly distributed on a square lattice of size 50 in dimensions 2 and 6. Samples were obtained by harvesting 20 realizations of 2500 points. Lower panels: model validation performed by comparing empirical and theoretical cdfs of the random variable  $n$ .

*Gaussian distribution* - Secondly, we tested the estimators on Gaussian distributed points in 5 dimensions. The standard deviation  $\sigma$  was set to 5 for each coordinate, implying an effective standard deviation of the distribution of  $\sigma_{eff} = \sqrt{d}\sigma$ . The points were projected on a lattice by taking the nearest integer in each coordinate. As one

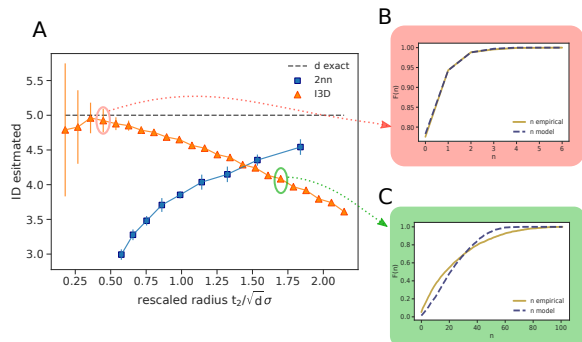


FIG. 2. ID estimation of I3D and 2nn on 20 realisations of 2500 points harvested from a gaussian distributions in 5d and projected on a lattice (A). Panels B and (C) show, respectively, the model validation at a small and large scales.

can observe in panel A of Fig.2, I3D is accurate as far as it explores a neighborhood in which the density does not vary too much (namely, as far as  $t_2/\sigma_{eff} \lesssim 1$ ). In this case there is in fact an almost perfect superposition of empirical and model cdfs in panel B. Beyond such distance, neighborhoods are characterised by non-constant density; consequently, the estimate gets less precise and, accordingly, the two cdfs show inconsistencies (panel C:  $t_2/\sigma_{eff} \sim 1.75$ ). We notice that also estimates at small radii, where the density should be approximately constant, are not perfectly matching the true intrinsic di-

mension and show large error bars. As in the previous case, this due to the low average abundance of points in the neighborhoods at small distances. *Spin dataset* - We also tested the I3D estimator on synthetic Ising-like spin systems with a tunable ID, which is given by the number of independent parameters used to generate the dataset. The 1d ensemble is obtained by generating a set of points belonging to a line embedded in  $\mathbb{R}^D$  with the process  $\varphi_i = \varphi_0 + \alpha\epsilon(i)$ . Here,  $\alpha$  is a fixed random vector of unitary norm with uniformly distributed components and  $\varphi_0 = -0.5$  is the y-intercept that, for simplicity, is equal for all the components;  $\epsilon_i$  are gaussian-distributed:  $\epsilon \sim \mathcal{N}(0, 10)$  and independently drawn for each sample  $i$ . We then proceed to the discretisation by extracting the  $z_i = \text{sign}(\varphi_i)$ , an ensemble of  $N$  states of  $D$  discrete spins. The pipeline is summarized in Fig. 3. The role of  $\varphi_0$  is to introduce an offset in order to enhance the number of the reachable discrete states. In fact, for  $\varphi_0 = 0$ , we would obtain only two different states, given by  $z = \text{sign}(\alpha\epsilon) = \pm \text{sign}(\alpha)$ , since the spins would change sign synchronously. An offset  $\neq 0$  implies that the different angles  $\varphi_i$  and the spins  $z_i$  shift sign in an asynchronous way. The extension to higher dimension is straightforward and consists in generating the initial points as  $\varphi_i = \varphi_0 + \sum_{j=1}^{id} \alpha_j \epsilon_j(i)$ , with  $\alpha_j \cdot \alpha_k \sim \delta_{jk}$ .

The I3D estimator is capable of inferring a meaningful ID across a wide range of distances (Panel A, bottom). We notice that the ID obtained with I3D is slightly lower than the true value. This is due to non-uniform density. For 1d and 2d systems, this effect is relatively small and indeed the empirical and theoretical cdfs are rather consistent (panels B and C). Such an effect becomes more important as the dimension rises (see SI for examples in  $d = 3$  and  $d = 4$ ).

The result of the I3D estimator on these toy systems is non trivial. Previous examples analyzed datasets explicitly built a on lattice where the features could assume any value in  $\mathbb{Z}$ , similarly to what happens in  $\mathbb{R}$ . Conversely, the spins' domain is defined by a Hamming graph<sup>18</sup>, corresponding to the vertices of an hypercube of size 1 and dimension  $D$ . There have been attempts<sup>19</sup> to explicitly map an Hamming graph onto a lattice. Here, instead, we infer the dimension of the lattice that would best accommodate the points of the dataset without performing the mapping explicitly. As we will show in the next example, this procedure can be carried out even if the embedding manifold is highly curved, and an explicit mapping can be performed only locally.

*16S Genomics strands* - Lastly, we present the application of our methodology to a real-world dataset in the field of genomics. The dataset consist of DNA sequences of  $\sim 100 - 300$  nucleotides. We selected a dataset downloaded from the Qiita server (<https://qiita.ucsd.edu/study/description/13596>)<sup>20</sup>. In such study they sequenced the v4 region of the 16S ribosomal RNA of the microbiome associated with the sponges and algal water blooms. This small-subunit of rRNA genes is widely used to study the composition of

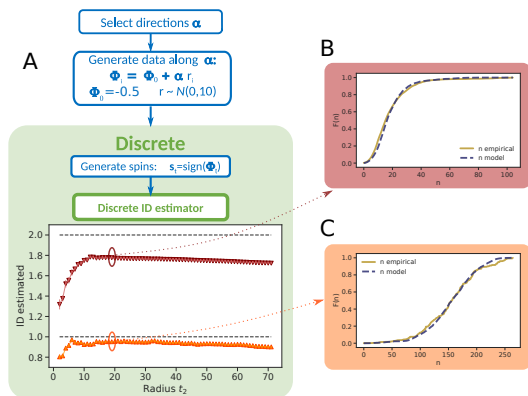


FIG. 3. (A) The pipeline used to create an ensemble of binary spins with a low ID, together with the results of the I3D estimator on 1d and 2d datasets. The estimation were validated through by comparing theoretical and empirical cdfs (panels B and C).

microbial communities<sup>21–24</sup>. Hamming distance and the binary mapping A:11, T:00, C:10 and G:01 were used to compute sequences’ distance. The canonical letter representation leads to almost identical results (see SI). To avoid dealing with isolated sequences, we kept only sequences having at least 10 neighbors within a distance of 10. Sequences come with their associated multiplicity, related to the number of times the same read has been found in the samples. We ignore such degeneracy and compute an ID which describes just the distribution of the points regardless of their abundance.

To begin with, we estimated the ID on a subset of sequences that are similar to each other. In order to find such sets, we perform a k-means clustering and calculate the ID separately for each of them. Panel A in Fig. 4 shows the ID at small to medium scale for one of such clusters. The empirical and reconstructed cdfs, performed at  $t_2 = 20$  (see inset), are fairly compatible. Panel B shows the average and the standard deviation of the ID of all clusters (weighted according to the respective populations). One can appreciate that the ID is always between 1 and 3 in a wide range of distances, showing a plateau around 2 for  $15 < t_2 < 40$ .

Such a low value for the ID is an interesting and unexpected feature, as it suggests that, despite the high-dimensionality of sequences’ space, evolution effectively operates in a low-dimensional space. Qualitatively, an ID of  $\sim 2$  on a scale of  $\sim 20$  means that if one considers all the sequences differing by approximately 20 mutations from a given sequence, these mutations cannot be consider independent one from each other, but are correlated in such a way that approximately 18 degrees of freedom are effectively forbidden. The “direction” of these correlated mutation can be, at least approximately, measured by performing PCA in the space of sequenced with the binary mapping. The first two dominant eigenvectors are shown in panel D, estimated for all the sequences within 20 (top) and 30 (bottom) from the center of the cluster

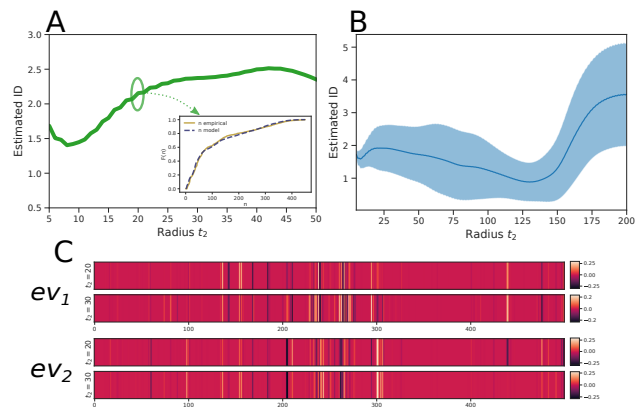


FIG. 4. Estimated ID at small to medium distances for one of the clusters of the genomics dataset (panel A). The inset reports the fair superposition of empirical and modeled cdfs of  $n$ . Panel B shows average and standard deviation of the IDs estimated separately for each cluster. Panel C shows first and second PCA eigenvectors of the data-points within a given distances  $t_2$  (20 or 30) from the center of cluster used for panel A.

of Panel A. Remarkably, the eigenvectors do not change significantly on this distance range, indicating that, consistently with the low value of the ID, the data manifold on this scale can be approximately described by a two-dimensional plane. In order to provide an interpretation of the vectors defining this plane, we repeated this same analysis on the previously mentioned spin model. In this case, if the generative model is defined by two vectors  $\alpha_1$  and  $\alpha_2$ , the first two dominant eigenvectors of a PCA performed with  $\sim 1000$  states are contained in the span of these vectors, with a residual of 0.04 (see SI for details). The components of a vector  $\alpha$  can then be qualitatively interpreted as proportional to the mutation probabilities of the associated nucleotide for a collective mutation process. In the genomics dataset this reasoning can applied only locally: the direction of correlated mutation is significantly different in different clusters, indicating that the data manifold is highly curved.

*Conclusions* - We presented an ID estimator formulated to analyze discrete datasets. Our method relies on few mathematical hypotheses and is asymptotically correct if the density is constant within the probe radius  $t_2$ . In order to prove the estimator’s effectiveness, we tested the algorithm against three different artificial datasets and compared it to a continuous-space estimator. While the latter, as expected, performed poorly, the former achieved good results in all cases, providing reliable ID estimations, corroborated by the comparison of empirical and model cumulative distribution functions for one of the observables. We finally applied the estimator on a genomics dataset, finding an unexpectedly low ID which hints at strong constraints in the sequences’ space, and then exploited such information to give a qualitative interpretation of such ID. The newly developed method paves the way to push the investigation even further, to-

wards the extension to discrete metrics of distance-based algorithms and routines that are, nowadays, consolidated in the continuum, such as density estimation methods or clustering algorithms.

The code implementing the algorithm is available in open source within the DADAp<sup>25</sup> software.

## I. ACKNOWLEDGEMENTS

The authors thank Antonietta Mira, Alex Rodriguez and Marcello Dalmonte for the fruitful discussions. AG and AL acknowledge support from the European Union’s Horizon 2020 research and innovation program (Grant No. 824143, MaX ‘Materials design at the eXascale’ Centre of Excellence).

IM, AG, AL designed and performed the research. All authors wrote the paper. JG designed the application on genomics sequences.

- <sup>1</sup>S. Solorio-Fernández, J. A. Carrasco-Ochoa, and J. F. Martínez-Trinidad, *Artificial Intelligence Review* **53**, 907 (2020).
- <sup>2</sup>A. Jović, K. Brkić, and N. Bogunović (*Ieee*, 2015) pp. 1200–1205.
- <sup>3</sup>Y. Bengio, A. Courville, and P. Vincent, *IEEE transactions on pattern analysis and machine intelligence* **35**, 1798 (2013).
- <sup>4</sup>T. Mendes-Santos, X. Turkeshi, M. Dalmonte, and A. Rodriguez, *Physical Review X* **11**, 011040 (2021).
- <sup>5</sup>T. Mendes-Santos, A. Angelone, A. Rodriguez, R. Fazio, and M. Dalmonte, *PRX Quantum* **2**, 030332 (2021).
- <sup>6</sup>A. Glielmo, B. E. Husic, A. Rodriguez, C. Clementi, F. Noé, and A. Laio, *Chemical Reviews* **121**, 9722 (2021), pMID: 33945269, <https://doi.org/10.1021/acs.chemrev.0c01195>.
- <sup>7</sup>A. Ansuini, A. Laio, J. H. Macke, and D. Zoccolan, *Advances in Neural Information Processing Systems* **32** (2019).
- <sup>8</sup>D. Doimo, A. Glielmo, A. Ansuini, and A. Laio, *Advances in Neural Information Processing Systems* **33**, 7526 (2020).
- <sup>9</sup>S. Recanatesi, M. Farrell, M. Advani, T. Moore, G. Lajoie, and E. Shea-Brown, *arXiv preprint* (2019).
- <sup>10</sup>P. Campadelli, E. Casiraghi, C. Ceruti, and A. Rozza, *Math. Probl. Eng.* **2015** (2015), 10.1155/2015/759567.
- <sup>11</sup>F. Camastra and A. Staiano, *Information Sciences* **328**, 26 (2016).
- <sup>12</sup>P. Grassberger and I. Procaccia, *Physical review letters* **50**, 346 (1983).
- <sup>13</sup>E. Ehrhart, *International Series of Numerical Mathematics*, Vol.35 (1977).
- <sup>14</sup>D. Moltchanov, *Ad Hoc Networks* **10**, 1146 (2012).
- <sup>15</sup>“Eugène ehrhart - publications 1947-1996,” [http://icps.u-strasbg.fr/~clauss/Ehrhart\\_pub.html](http://icps.u-strasbg.fr/~clauss/Ehrhart_pub.html), accessed: 2022-03-25.
- <sup>16</sup>M. Beck and S. Robins, *Choice Reviews Online* **45**, 45 (2007).
- <sup>17</sup>E. Facco, M. D’Errico, A. Rodriguez, and A. Laio, *Scientific Reports* **7**, 1 (2017).
- <sup>18</sup>“Hamming graph,” [https://en.wikipedia.org/wiki/Hamming\\_graph](https://en.wikipedia.org/wiki/Hamming_graph) (2022), accessed: 2022-04-11.
- <sup>19</sup>E. Wilkeit, *Journal of Combinatorial Theory, Series B* **50**, 179 (1990).
- <sup>20</sup>E. Bolyen et al., *Nature Biotechnology* **37**, 852 (2019).
- <sup>21</sup>M. W. Gray, D. Sankoff, and R. J. Cedergren, *Nucleic Acids Research* **12**, 5837 (1984).
- <sup>22</sup>C. R. Woese, O. Kandler, and M. L. Wheelis, *Proceedings of the National Academy of Sciences* **87**, 4576 (1990).
- <sup>23</sup>W. G. Weisburg, S. M. Barns, D. A. Pelletier, and D. J. Lane, *Journal of bacteriology* **173**, 697 (1991).

<sup>24</sup>J. Jovel, J. Patterson, W. Wang, N. Hotte, S. O’Keefe, T. Mitchel, T. Perry, D. Kao, A. L. Mason, K. L. Madsen, et al., *Frontiers in microbiology* **7**, 459 (2016).

<sup>25</sup>A. Glielmo, I. Macocco, D. Doimo, M. Carli, C. Zeni, R. Wild, M. d’Errico, A. Rodriguez, and A. Laio, “Dadapy: Distance-based analysis of data-manifolds in python,” (2022).

Intrinsic dimension estimation for discrete metrics  
— Supplementary Information —

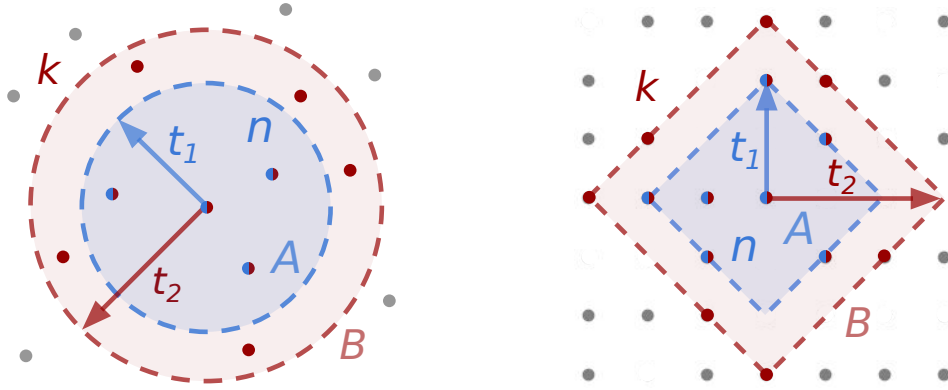


FIG. 5. Sketchy representation of hyperspheres for the typical  $L^2$  metric in continuous spaces (left) and for lattices (right). In order to find the ID we exploit the binomial relationship between the  $n$  (blue) points within region  $A$  -of radius  $t_1$ - and  $k$  (red) points within region  $B$  -of radius  $t_2$ -. Points within the inner region  $A$  count for both  $n$  and  $k$ .

## II. PROOF OF EQ.(2)

We recall that

$$\begin{aligned}
 P(n, A) &= \frac{[\rho V(A)]^n}{n!} e^{-\rho V(A)} \\
 P(k, B) &= \frac{[\rho V(B)]^k}{k!} e^{-\rho V(B)} \\
 P(k-n, V(B \setminus A)) &= \frac{[\rho V(B \setminus A)]^{k-n}}{(k-n)!} e^{-\rho V(B \setminus A)}
 \end{aligned} \tag{8}$$

where we name  $\lambda_1 = \rho V(A)$  and  $\lambda_2 = \rho V(B \setminus A)$ , so that  $\lambda_1 + \lambda_2 = \rho(V(A) + V(B \setminus A)) = \rho V(B)$  since  $A \subset B$ . Consequently it holds that

$$\begin{aligned}
 P(n | k) &= \frac{P(n, k)}{P(k)} = \frac{P(n)P(k-n)}{P(k)} = \\
 &= \binom{k}{n} \left( \frac{\lambda_1}{\lambda_1 + \lambda_2} \right)^n \left( \frac{\lambda_2}{\lambda_1 + \lambda_2} \right)^{k-n} = \\
 &= \binom{k}{n} p^n (1-p)^{k-n}
 \end{aligned} \tag{9}$$

where  $p = \frac{V(A)}{V(B)}$ .

## III. EHRHART POLYNOMIAL THEORY AND CROSS-POLYTOPE ENUMERATING FUNCTION

According to Ehrhart theory, the volume of a lattice hypersphere of radius  $t$  in  $d$  dimension is given by the enumerating function<sup>16</sup>

$$V_{\circlearrowleft}(t, d) = \sum_{k=0}^d \binom{d}{k} \binom{t-k+d}{d}. \tag{10}$$

where  $d$  is assumed to be an integer value. In order to make this expression suitable for likelihood maximization, it can be conveniently rewritten using the analytical continuation

$$V_{\diamond}(t, d) = \binom{d+t}{d} {}_2F_1(-d, -t, -d-t, -1) \quad (11)$$

where the binomial coefficient, for a non-integer  $n$  are computed using the Gamma function:  $n! = \Gamma(n+1)$ .  ${}_2F_1$  is the hypergeometric function. Here we report the first polynomials for  $t \leq 4$ :

$$t = 0: 1$$

$$t = 1: 1 + 2d$$

$$t = 2: 1 + 2d + 2d^2$$

$$t = 3: 1 + \frac{8}{3}d + 2d^2 + \frac{4}{3}d^3$$

$$t = 4: 1 + \frac{8}{3}d + \frac{10}{3}d^2 + \frac{4}{3}d^3 + \frac{2}{3}d^4$$

By substituting integer values of  $d$ , one recovers the volumes found with eq. 10. Using this expansion we can treat  $d$  as a continuous parameter in our inference procedures.

#### IV. MAXIMUM LIKELIHOOD ESTIMATION OF THE ID

Once the two radii  $t_1$  and  $t_2$  are fixed and the corresponding values of  $n_i$  and  $k_i$  are computed, the likelihood for  $N$  data points is

$$\mathcal{L}\{d|(n_i, k_i)\} = \prod_i^N \text{Binomial}(n_i; k_i, p(d)) = \prod_i^N \binom{k_i}{n_i} (p(d))^{n_i} (1-p(d))^{k_i-n_i} \quad (12)$$

where  $p(d) = V_{\diamond}(t_1, d)/V_{\diamond}(t_2, d)$  and depends explicitly only on  $d$ . In order to make the expressions easier to read, we will write just  $p$  from now on. In order to find the optimal value for  $d$ , one can perform a maximum likelihood estimation (MLE), which consists in setting equal to 0 the (log)derivative of the likelihood:

$$\begin{aligned} 0 &= \frac{\partial}{\partial d} \ln(\mathcal{L}) = \sum_i^N \frac{\partial}{\partial d} \ln(\text{B}(n_i; k_i, p)) = \\ &= \sum_i^N \frac{\partial}{\partial d} (n_i \ln(p) + (k_i - n_i) \ln(1-p)) = \\ &= \sum_i^N \left( n_i \frac{p'}{p} - (k_i - n_i) \frac{p'}{1-p} \right) = \\ &= \langle n \rangle \frac{p'}{p} - (\langle k \rangle - \langle n \rangle) \frac{p'}{1-p} \end{aligned} \quad (13)$$

where the mean value are intended over all the points of the dataset and  $p' = dp/dd$  is the Jacobian of the transformation from  $p$  to  $d$ , which reads

$$\frac{d}{dd} \frac{V_{\diamond}(t_1; d)}{V_{\diamond}(t_2; d)} = \frac{V'_{\diamond}(t_1)V_{\diamond}(t_2) - V_{\diamond}(t_1)V'_{\diamond}(t_2)}{V_{\diamond}(t_2)^2}. \quad (14)$$

The last line of Eq. (13) leads directly to equation (6).

##### A. Cramer-Rao estimate of the variance of the ID

The Cramer-Rao inequality states that the variance of an unbiased estimator of an unknown parameter is bounded from below from the inverse of the Fisher information, namely

$$\text{Var}(\hat{\theta}) \geq \frac{1}{\mathcal{I}(\theta)} \quad (15)$$

where

$$\mathcal{I}(\theta) = N\mathbb{E} \left[ \left( \frac{\partial}{\partial \theta} \ln \mathcal{L}(x; \theta) \right)^2 \right] = -N\mathbb{E} \left[ \frac{\partial^2}{\partial \theta^2} \ln \mathcal{L}(x; \theta) \right], \quad (16)$$

$\mathcal{L}$  is the likelihood for a single sample  $x$  and  $\mathbb{E}$  is the expected value over  $x$ . Given the likelihood in eq. (12) and deriving with respect to  $d$  a second time the third line of eq.(13), we obtain

$$\frac{\partial^2}{\partial d^2} \ln \mathcal{L}(d; n_i) = \sum_i^N \left( p'' \left( \frac{n_i}{p} - \frac{k_i - n_i}{1-p} \right) + p' \left( -p' \frac{n_i}{p^2} - p' \frac{k_i - n_i}{(1-p)^2} \right) \right). \quad (17)$$

By inserting the MLE solution  $\langle n \rangle = p\langle k \rangle$  and by performing the sum one obtains

$$\frac{\partial^2}{\partial d^2} \ln \mathcal{L}(d; n_i) = -N\langle k \rangle \frac{p'^2}{p(1-p)}, \quad (18)$$

leading to the final result

$$\text{Err}(d; t_1, t_2, N) \geq \sqrt{\frac{p(1-p)}{\langle k \rangle N p'^2}} \Big|_{d=d_{MLE}}. \quad (19)$$

Such an expression is finally evaluated at the  $d$  found through the MLE procedure.

## V. BAYESIAN ESTIMATE OF THE ID

The ID can also be estimated through a Bayesian approach. The likelihood of the process is represented by a binomial distribution where the probability  $p$  (hereafter named  $x$  to avoid confusion) is given by the ratio of the shell volumes around any given point. The binomial pdf has a known conjugate prior: the beta distribution, whose expression is

$$\text{Beta}(x; \alpha, \beta) = \frac{x^{\alpha-1}(1-x)^{\beta-1}}{\mathcal{B}(\alpha, \beta)}, \quad (20)$$

where  $\mathcal{B}$  is the beta function. We make an agnostic assumption (since we do not have any information on the value of the ID) and set  $\alpha = \beta = 1$ , so that  $x$  will be uniformly distributed. The posterior distribution of the ratio of the volumes  $x$  will still be a Beta distribution, with parameters updated as follows

$$\alpha = \alpha_0 + \sum_{i=1}^N n_i \quad (21)$$

$$\beta = \beta_0 + \sum_{i=1}^N (k_i - n_i) \quad (22)$$

where  $n_i$  and  $k_i$  are the points falling within the inner and outer volumes around point  $i$  and the sum runs on all the points in the dataset.

In order to compute the expected value and the variance on  $d$ , one has to extract its posterior distribution  $P(d)$  from the one of  $x$ . The posterior of  $d$  is obtained from the posterior of  $x$  by a simple change of variables:

$$P(d) = P(p(d)) \left| \frac{dp}{dd} \right| = \text{Beta}(p; \alpha, \beta) \left| \frac{dp}{dd} \right| \quad (23)$$

where the Jacobian is given by Eq. (14). By varying  $d$ , one can estimate the posterior distribution of  $d$ . Its first and second momenta will be the (Bayesian) estimates of the ID and of its confidence.

As far as we could observe, the ID found through MLE is always very close to the mean value of the posterior. The same occurs for the error estimate, which is typically very close to the Cramer-Rao bound. Small differences ( $< 1\%$ ) have been observed in cases of few datapoints ( $\sim 50$ ). The reason is that the posterior distribution, for low values of  $\alpha$  and  $\beta$ , can be slightly asymmetric, bringing to a discrepancy between the position of its maximum and its mean value. In most practical cases such an effect is negligible.



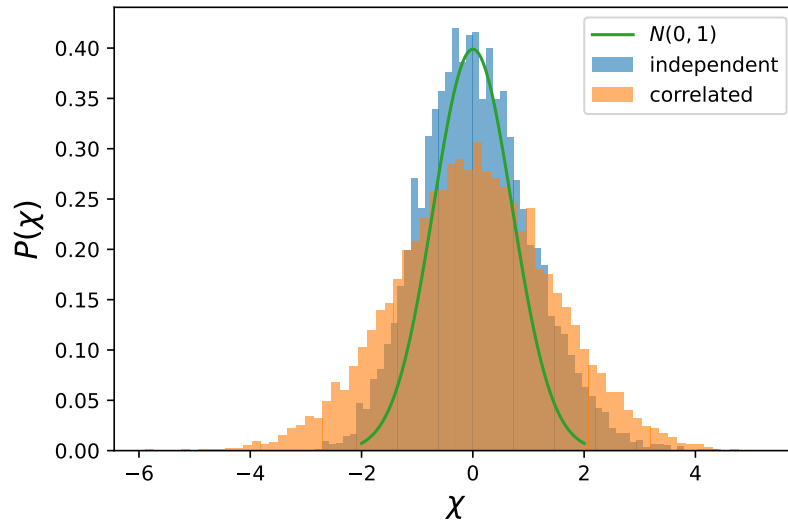


FIG. 6. The pool distributions (see text) show that the correlation between the neighbourhoods of the points brings to an error estimate which slightly underestimates the value that would be obtained using statistically independent samples.

## VI. STATISTICAL CORRELATION IN THE NUMBERS OF DATA POINTS IN THE PROBE REGIONS.

The likelihood has the form in Eq. 12 under the assumption that the observations  $n_i$  are statistically uncorrelated. However, if a point  $j$  is close to another point  $i$ , it is likely that their neighborhoods will be overlapping. This implies that the values for  $n_i$  and  $n_j$  will have a certain degree of correlation. In particular, in order to have a fully statistical independence, one should consider only points with a non-overlapping neighbours. Clearly this would reduce the number of available observations to compute the ID, making the estimate less reliable. Here we assess the entity of such correlations, or seemingly, how much the Bayesian and Cramer-Rao calculations underestimate the error.

To begin with, we generated 10000 realizations of 10000 uniformly distributed points on a 4-dimensional lattice. For each realization, we extracted ID and error using all available points; on the same dataset, we also computed the ID using only one random point, in order to gather statistically independent measurements. We then computed the distribution of the pool variable for the correlated ID measures as

$$\chi_{corr} = \frac{d_{cor} - d_{gt}}{\sigma_{Bayes}}, \quad (24)$$

where  $\sigma_{Bayes}$  is the standard deviation of the posterior, and  $d_{gt}$  is the ground truth ID. We also computed the distribution of the pool variable for the ID estimates obtained using a single point

$$\chi_{ind} = \frac{d_{ind} - d}{\sigma_{stat}}, \quad (25)$$

where  $\sigma_{stat}$  is the standard deviation of the distribution of the single-point ID estimates. We expect  $\chi_{ind} \sim \mathcal{N}(0, 1)$  and that's what we obtained as shown from the blue histogram in Fig. 6. On the other hand, the distribution obtained for the pool of correlated measurements  $\chi_{cor}$  (orange histogram in Fig. 6) shows a higher spread, indicating that the  $\sigma_{Bayes}$  systematically underestimate the error of the  $\sim 30\%$ . This was expected, as both the Bayesian and likelihood formulation assume to sample statistically independent observations. We can then conclude that the statistical dependence of neighborhoods in the calculation of ID leads to an error estimate which is slightly below the correct value but it is still very indicative.

## VII. ANALYTICAL RESULTS IN CONTINUUM SPACE

The ID estimation scheme proposed in our work can be easily extended and applied to different metrics than the lattice one, used to build the I3D. In particular, within any  $L^p$  metric in the continuum space, the volume of the

hyper-spheres scales as a canonical power law of the radius multiplied by a prefactor depending on both the dimension  $d$  and the value  $p$ :

$$V_d^p(R) = \frac{(2\Gamma(\frac{1}{p} + 1)R)^d}{\Gamma(\frac{d}{p} + 1)} = \Omega_d^p R^d.$$

As a consequence, the ratio of volumes that occurs in the binomial distribution of eq. (3) becomes

$$p(r, d) = \frac{\Omega_d R_1^d}{\Omega_d R_2^d} = \left(\frac{R_1}{R_2}\right)^d = r^d. \quad (26)$$

Because of the well-behaved scaling of the volume with the radius in continuous metrics, all the formula presented so far in the discrete case simplify a lot, allowing for further analytical derivations concerning both the MLE and Bayes analyses, as shown in the two following sections.

### A. Maximum Likelihood Estimation and Cramer-Rao lower bound

In the continuum case, given the previous expression for the ratio of volumes, the MLE and Cramer-Rao relations can be utterly simplified from Eq. (6) so that we can obtain an explicit form for the intrinsic dimension. Concretely, by substituting  $p = r^d$  into eq. (6) we find

$$d = \frac{\ln(\langle n \rangle / \langle k \rangle)}{\ln(r)} \quad (27)$$

for the MLE, while the Cramer Rao inequality (19) becomes

$$\text{Var}(d; r, N, k) \geq \frac{1 - r^d}{\langle k \rangle N \ln(r)^2 r^d}. \quad (28)$$

In order to have an estimate as precise as possible, we are interested in the value of  $r$  that minimize the variance. Being (28) a convex function, we find a single minimum that corresponds to

$$r_{opt}(d) = 2^{-1/d} \left( -W \left( -\frac{2}{e} \right) \right)^{1/d} \approx 0.2032^{\frac{1}{d}} \quad (29)$$

where  $W$  is the Lambert  $W$  function. Of course in principle we don't know the intrinsic dimension of the system, and thus we don't have a direct way to practically select  $r_{opt}$  if not through successive iterations. This relationship tells us that higher  $d$  needs higher  $r$  to provide a better estimate. The above relation also suggests that the optimal ratio between the points in the two shell should approach  $\langle n \rangle / \langle k \rangle \sim r_{opt}^d = 0.2032$ . This implies that there is an optimal and precise fraction of points, and thus volumes, for which the estimated ID is more accurate. Supposing that we are able to find such  $r_{opt}$ , we might ask how the variance scales with the dimensionality of the system. We obtain that

$$\text{Var}(d; r_{opt}, N, k) = \frac{1 - r_{opt}^d}{\ln(r)^2 k N r_{opt}^d} \propto \frac{d^2}{Nk} \quad (30)$$

This implies that the precision of our estimator scales with the square of the dimension.

### B. Bayes formulation

Also the Bayesian computations in the continuum case allows for analytical results. In particular, from eq. (23), one obtains

$$p(d) = \text{Beta}(r^d; \alpha, \beta) |r^d \ln(r)|. \quad (31)$$

From this expression one can easily derive the first and second momenta of the distribution. In particular, performing the change of variable  $d = \ln x / \ln r$ , we have

$$\langle d \rangle = \int_0^\infty dd p(d) d = -\frac{1}{\ln(r)} \int_0^1 dx \text{Beta}(x; \alpha, \beta) \ln(x) = \frac{\psi_0(\alpha) - \psi_0(\alpha + \beta)}{\ln(r)} = \frac{\psi_0(1 + \sum_{i=1}^N n_i) - \psi_0(2 + \sum_{i=1}^N k_i)}{\ln(r)} \quad (32)$$

where  $\psi_0(z) = \frac{d}{dz} \ln \Gamma(z)$  is the digamma function and in the last passage we have inserted the definitions for  $\alpha$  and  $\beta$  (22). Exploiting the same change of variable, also the variance shows a simple expression:

$$\text{Var}(d) = \frac{\text{Var}(\ln(x))}{\ln(r)^2} = \frac{\psi_1(\alpha) - \psi_1(\alpha + \beta)}{\ln(r)^2} = \frac{\psi_1(1 + \sum_{i=1}^N n_i) - \psi_1(2 + \sum_{i=1}^N k_i)}{\ln(r)^2} \quad (33)$$

where  $\psi_1(z) = \frac{d^2}{dz^2} \ln \Gamma(z)$  is the trigamma function.

### VIII. SPIN SYSTEMS

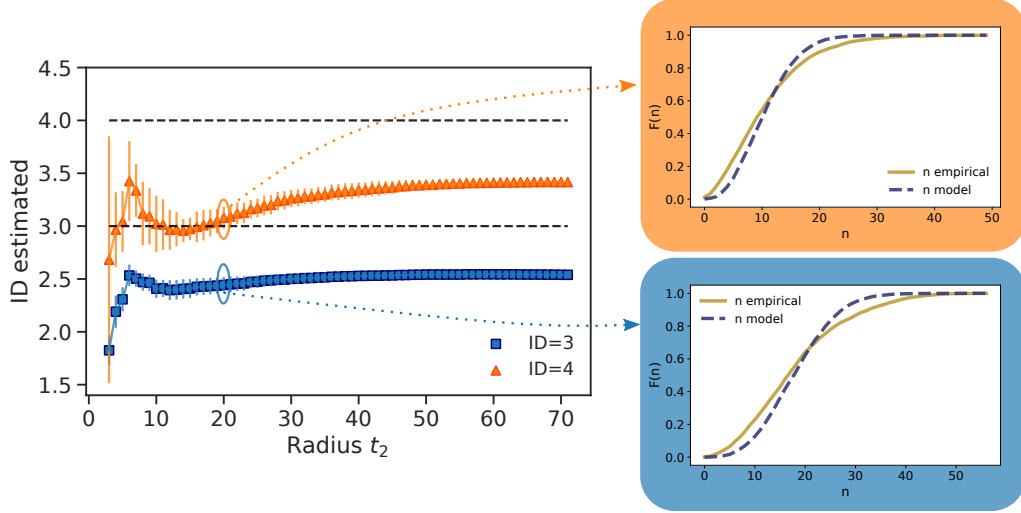


FIG. 7. The I3D estimator underestimates the ground truth ID of spin systems in the case of  $d = 3$  and  $d = 4$ . The inconsistency is shown by the model validation plots, where theoretical and empirical cdf are not well superimposed.

#### A. PCA on discrete spins

Here we address the possibility of performing PCA on discrete datapoints, justifying the results of the last section. We start from recalling that the continuous spins were generated using a linear embedding  $\varphi_i = \varphi_0 + \alpha \epsilon(i)$ , so that it is possible to retrieve the directions of the generating vectors  $\alpha_i$  using standard PCA and a number of points  $N \geq \text{ID} + 1$ .

In the case of spin states retrieving the value of  $\alpha$  is not so straightforward. In particular, two spin states differ from each other by a finite (and possibly very small) amount of spin flips. This means that we have a piece of information only on a fraction of the features, namely the varying spins. For this reason we need many more points in order to gather statistics about the behaviour of the spins and how often they flip across the dataset. The idea is that PCA eigenvectors can capture the frequency of spin flips and give a proxy of the embedding directions  $\alpha_i$ . The result for ID=1 is reported in Fig. 8 and compares the generating vector  $\alpha$  and the first PCA eigenvector  $v_1$ . The overlap is almost perfect, and we have  $\alpha \cdot v_1 \sim 0.98$ . In higher dimensions the eigenvectors will be rotated with respect to the



FIG. 8. Comparison of the embedding vector  $\alpha$  and the first PCA eigenvector  $v_1$  obtained with  $\sim 1000$  points in the 1-dimensional case. The overlap is almost perfect:  $\alpha \cdot v_1 \sim 0.98$ .

original embedding vectors, so that a direct visual comparison cannot be made as in the previous case. Hence, we

estimate the residual of the overlap, defined as

$$\mathcal{R} = d - \sum_{i,j=1}^d (\alpha_i \cdot v_i)^2. \tag{34}$$

In the 2-dimensional case, we find that  $\mathcal{R} \sim 0.04$ , meaning that, like for the 1-dimensional example, we are able to retrieve  $\sim 98\%$  of the generative process information.

**IX. RESULTS FOR DIFFERENT NUCLEOTIDE SEQUENCE DISTANCES**

One might wonder how the ID estimate depends on the metric used to compute the distance between sequences. As, anticipated in the main text, we considered two possible mappings. The first one maps each letter to a two spin state as follows: A:11, T:00, C:10 and G:01. The distance is then measured through Hamming or Manhattan indifferently. As a consequence complementary purine and pyrimidine are at distance 2, while other distances are just 1. The other possibility is to use the Hamming distance straightly on the sequences as they are, meaning that all nucleotides are equidistant one from the other. Fig. 9 shows the ID as a function of the scale of the same cluster used in the main text. The behaviour of the ID depends very slightly on the chosen distance measure. For this reason we decided to stick to the spin mapping, as it allows retrieving the local "directions" of the generating process by a PCA analysis.

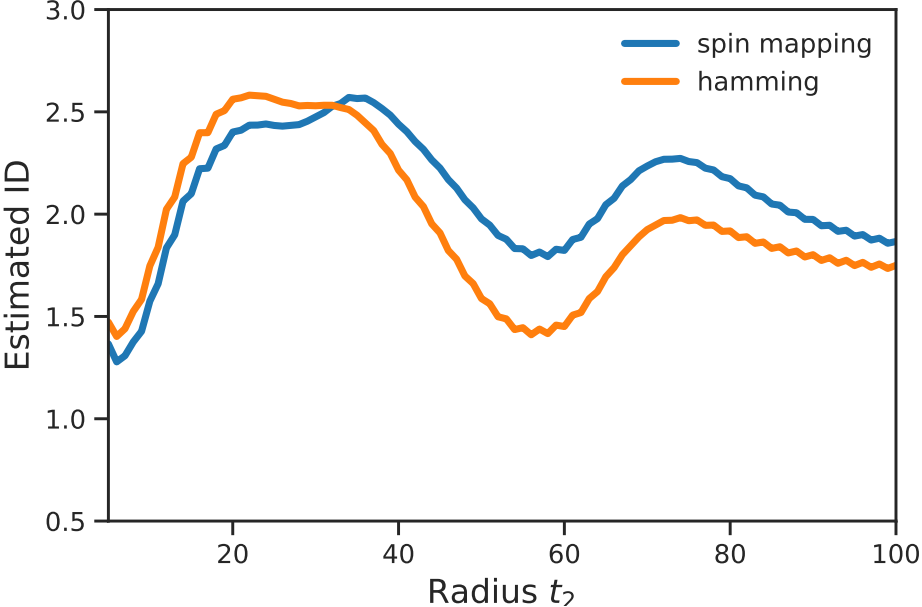


FIG. 9. The metric chosen to calculate distances between sequences is basically irrelevant when computing the ID.